Journal of the Earth and Space Physics, Vol. 45, No. 4, Winter 2020, P. 121-131
DOI: 10.22059/jesphys.2019.269596.1007065

Combination of Artificial Neural Network and Genetic Algorithm to Inverse Source Parameters of Sefid-Sang Earthquake Using InSAR Technique and Analytical Model Conjunction

Haji Aghajany, S.[1], Pirooznia, M.[1], Raoofian Naeeni, M.[2*] and Amerian, Y.[2]

1. Ph.D. Student, Department of Geodesy, Faculty of Geodesy and Geomatics Engineering, K. N. Toosi University of Technology, Tehran, Iran
2. Assistant Professor, Department of Geodesy, Faculty of Geodesy and Geomatics Engineering, K. N. Toosi University of Technology, Tehran, Iran

(Received: 1 Dec 2018, Accepted: 14 May 2019)

Abstract
In this study, an inversion method is conducted to determine the focal mechanism of Sefid-Sang fault by comparing interferometric synthetic aperture radar (InSAR) technique and dislocation model of earthquake deformation. To do so, the Sentinel-1A acquisitions covering the fault and its surrounding area are processed to derive the map of line of sight (LOS) displacement over the study area. Then, using the ascending and descending tracks of the satellite, the three-dimensional displacement field is recovered over the region. The maximum horizontal and vertical displacements are about 12 cm and 5 cm respectively. The resulting displacement field is compared with Okada half-space dislocation model of earthquake to determine the focal mechanism and fault parameters by a nonlinear inversion method, which is composed of artificial neural network (ANN) and genetic algorithm (GA). The coulomb stress and strain changes, which are important factors for prediction of aftershock event, are also determined. The numerical achievements show a slip of 4.5 mm, a depth of 8 km, dip angle of 55 deg and width of 10 km for this fault.

Keywords: InSAR, Okada, ANN, GA, Sefid-Sang earthquake, Fault parameters, Coulomb stress.

1. Introduction
Surface deformation measurements are the important means of monitoring and understanding the crustal deformation related to a variety of geophysical phenomenon (Zebker and Villasenor, 1992). These measurements have been widely used to study both natural and man-made processes such as earthquake, magmatic flow in volcanic systems, landslide, glacial flow, and subsidence due to the ground water extraction (Fattahi and Amelung, 2016; Xu et al., 2010). Recently, InSAR technology has been extensively used to measure the deformation field triggered by rupture on the dislocation surfaces of the faults, particularly for the study of co-seismic deformations, which may have a significant magnitude (Fialko et al., 2001; Motagh et al., 2015). SAR interferometric data can also be used to extract the three dimensional (3D) deformation of the Earth's surface by using the phase part of the radar signal. In addition to observational techniques such as InSAR and Global Positioning System (GPS) (Wang et al., 2013; Haji-Aghajany et al., 2017) which measure the amount of deformation, there are different analytical models that investigate the physical nature of the deformation to conceive its relation with the tectonic activities within the Earth. In a relation to seismic displacements, the elasticity theory of dislocation plays an important role in characterizing the mechanism of earthquake, which relates the deformation field to the geometric parameters of the faults and the physical properties of an earthquake source. The study of co-seismic deformation in a half-space, spherical and layered Earth model has been the subject of many scientific researches (Kawasaki et al., 1995; Furuya and Satyabala, 2008; Kaneko et al., 2013). The half-space Earth model that was first introduced by Steketee (1958a, b), and later developed by Maruyama (1964), and Okada (1985), has become a standard model for the study of earthquake source parameter. Okada (1985) derived the 3D deformation field due to a slip on the surface of rectangular fault buried in a homogeneous and isotropic half-space.

On Wednesday, 05 April 2017, the

*Corresponding author: mraoofian@kntu.ac.ir

earthquake with magnitude 6.1 M_w was triggered at 3 km from the Sefid-Sang city and 84 km from southeast of Mashhad city, in Khorasan Razavi province of Iran. According to seismic records of the Institute of Geophysics at the University of Tehran, the cause of this earthquake was the Sefid-Sang fault whose foci was located at a depth of 6 km. According to the report from this institute, the Sefid-Sang earthquake has been the result of a reverse fault, in which the compressive stress between the two sides of the fault produced the dip-slip dislocation. Fig. 1 shows the earthquake center and the study area. Mashhad city is the second largest city in Iran. It is located in northeastern of Iran surrounded by active seismic zones. It has experienced several destructive earthquakes in the history of seismology of Iran, and thus there is the possibility of powerful events in this area and around it. This active tectonic region is located in the Mashhad Plain, between Kopet-Dagh basin in the north and Binaloud mountain range in the south, both of which have the potential for large and strong earthquakes. The Plain was formed by tectonic movements of several faults, which extend along the northwest to the southeast (Ambraseys and Melville, 1982; Akbari et al., 2011). On the basis of the recent studies conducted by the International Institute of Earthquake Engineering and Seismology (IIEES), it has been pointed out that the tectonics of the area has a quite complex structure (Walker et al., 2003). In Fig. 1, seismic hazard zonation map of the study area based on iso-acceleration contours for a return period of 75 years has been shown. According to this map, the area is located in a medium to high hazard zone. Among the powerful earthquakes that have occurred in this area, one can mention the significant earthquakes of 1598, 1676 and 1678 A.D (Akbari et al., 2011). The most important historical earthquake was that on July 30, 1673, which killed about 4,000 people (Ambraseys and Melville, 1982; Akbari et al., 2011).

In this study, an inversion method is conducted to obtain the fault parameters of the 2017 Sefid-Sang earthquake using InSAR co-seismic deformation fields in a conjunction with the analytical model of Okada (1985). To do so, the Sentinel-1A acquisitions for both descending and ascending tracks of the satellite are processed to determine the 3D displacement field over the study area. After determination of the actual displacement field due to the fault rupture, it is entered into the analytical model of Okada (1985) to constrain the fault parameters and focal mechanism of this earthquake. Specifically, the nonlinear inversion algorithm that includes the combination of ANN and GA, is applied to tackle the seismic inverse problem. Since the earthquake could change the coulomb stress near the fault planes, and then make the aftershocks easier to occur or delayed to occur, the coulomb stress as an important seismological factor is also computed at the fault plane and its spatial variation is discussed.

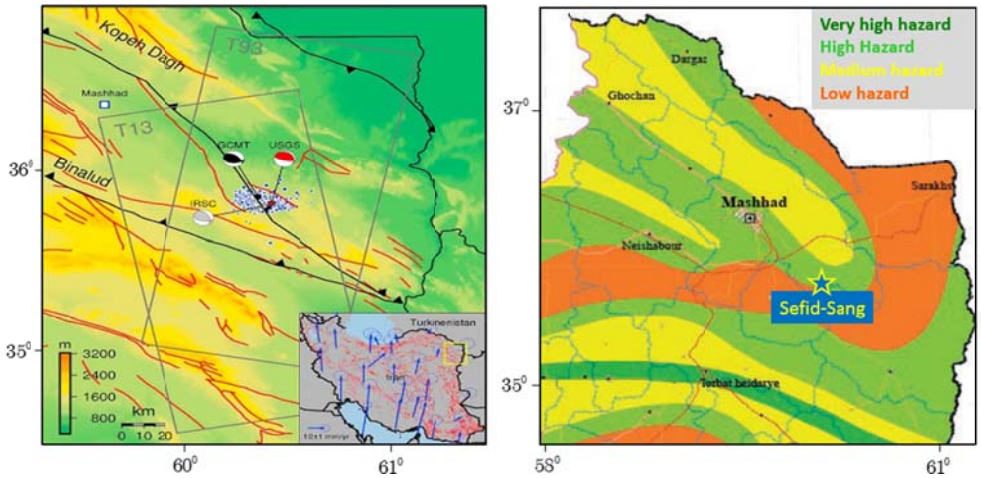

Figure 1. Earthquake center and its surrounding region and seismic hazard zonation map of the study area (Akbari et al., 2011; Guangyu et al., 2018).

2. InSAR techniques for the measurement of deformation

The InSAR technique can measure the projection of the deformation vector onto the LOS direction, defined as the shortest path from a given point on ground to the SAR antenna phase center. InSAR provides some unique capabilities for the study of crustal deformation and active processes (Huadong et al., 2010). The basic InSAR observable is called an interferogram, which represents the per-pixel phase difference between two SAR acquisitions. For a given interferogram, the observed InSAR phase change can be expressed as (Jolivet et al., 2012; Wang et al., 2013):

$$\Phi = \Phi_{def} + \Phi_{topo} + \Phi_{atm} + \Phi_{Flatten} + \Phi_{noise} \quad (1)$$

where Φ_{def} is the deformation phase along the LOS direction, Φ_{topo} is the phase resulted from the topography effect, Φ_{atm} is the phase resulted from the atmospheric delay, $\Phi_{Flatten}$ is the phase from the orbital effect and Φ_{noise} is the phase related to other thermal noise errors (Zebker and Villasenor, 1992). Since we decide to extract the displacement field from InSAR observations, namely, Φ_{def} , the other contributions in the observable InSAR phase should be modeled from auxiliary data and removed from Eq. (1).

In this study, for the reduction of the topography and orbital effects, the Aster DEM with resolution of 30 m and orbital files are used respectively. Orbital data are not accurate enough to remove the orbital effects completely. It has been proved that in coseismic studies, these residuals represent one or two fringes at most. If these residuals cannot be ignored, it must be removed using the best fitting twisted plane. The authors did this process and the result showed that these residuals can be discarded.

The measured LOS displacement u_{LOS} represents the projection of the vector displacement field U(U_e , U_n ,U_u) onto the LOS vector in which (Fialko et al., 2001):

$$[U_n \sin\varphi - U_e \cos\varphi]\sin\lambda + U_u \cos\lambda + \delta_{los} = u_{los} \quad (2)$$

where φ is the azimuth of the satellite heading vector, λ is the radar incidence angle at the reflection point and δ_{LOS} is the measurement error. The azimuthal offset u_{AZO} is a projection of the horizontal component of the displacement vector onto a satellite heading vector (Fialko et al., 2001) which can be written as

$$[U_n \cos\varphi - U_e \sin\varphi] + \delta_{azo} = u_{AZO} \quad (3)$$

For each pixel of the InSAR data, a linear system of two equations for the LOS displacements from the ascending and descending orbits, combined with one equation for the azimuthal offsets of the descending orbit are used to determine the three components of the displacement vector (Fialko et al., 2001).

3. Analytical model of earthquake deformation

Okada (1985) is one of the simplest analytical models for investigation of surface deformation due to rupture on a fault surface. The motion of a fault can be caused by various dislocations. Okada (1985) prepared an analytical expression for the surface displacement, strain and tilt. This model computes displacement field in 3D space as a function of fault parameters. Consequently, with the presence of real displacement field obtained by observational methods such as InSAR, and comparison with displacement fields obtained from the Okada model, the parameters of the fault can be determined from the solution of an inverse problem.

4. ANN equipped with GA

Determination of fault parameters by inversion of Okada model using InSAR displacement field is actually a kind of nonlinear least square adjustment problem. Thus, the use of proper optimization method for solution of this problem is an inevitable task (Haupt and Haupt, 2004). Generally, the optimization method can be classified into two groups: classical and evolutionary methods. Classical methods such as steepest descent, conjugate gradient and so on use mathematical functions and their derivatives to obtain the optimum point. These methods are dependent on the correct initial values

and they are very sensitive to the choice of initial setup. Moreover, due to the use of function derivatives, they have some difficulties with complicated functions such as those that are dealt with in this study. Since the performance of these algorithms is highly dependent on the choice of initial values, it is most likely that they find a local optimum point instead of a global one (Haupt and Haupt, 2004) in the cases that the initial setup does not choose correctly.

Unlike the classical methods, evolutionary optimization methods such as ANN and GA use intelligent algorithms to find the solution. Therefore, the evolutionary methods do not have the problem of being trapped in a local optimum point, because they do not depend on the exact values of initial parameters (Del Frate and Salvatori, 2004; Haupt and Haupt, 2004).

ANN is one of the most applicable evolutionary optimization methods in nonlinear optimization, signal processing, intelligent control and so on. This method is a kind of combination of computer science and biology. ANN has a computational structure of biological neuron systems that can discover and resolve nonlinear and complex relationships between inputs in order to find a global optimum point in a large and finite space (Zell et al., 1995; Del Frate et al., 2003; Del Frate and Salvatori, 2004). The ANN consists of many nodes called neurons that communicate with each other using node connections called synapses. ANN has three main layers: input, output, and hidden. In the processing with ANN, two factors play an important role in the accuracy of the results: The interconnecting weights in the structure of the ANN and their modified quantities. Synapse weights the value sent from a connected neuron. Weights may have a positive, negative, or zero values. These values may be integer or real numbers depending on the application of ANN. Because of the lack of information, the initial weights of ANN are often produced stochastically (Yang et al., 2001). Estimating the initial weights that are global is difficult. Improper choice of weights might cause the ANN to be trapped in a local minimum and thus decreases the probability of finding the global optimum point. Moreover, it can reduce the convergence velocity of method and in some cases it may not converge at all. These limitations in artificial neural network must be resolved and optimized (Yang et al., 2001).

Because of the above-mentioned drawbacks, in this study, GA is used to produce the weights of the network connection of ANN optimization process. GA is a global iterative optimization method in which, by simulating the evolutionary processes of organisms, especially selection and elimination, the colony is selected and mutated repeatedly (Wang and Cao, 2002). One of the most important laws of evolution and mutation is the survival of the best and elimination of the worst (Wang and Cao, 2002). Based on these laws, as well as the adaptive estimation of every individual, better colony is gradually produced. The best individuals in the optimized colony are also found by global and parallel techniques (Goldberg, 1989; Michalewicz, 1992). GA has very strong ability of global searching, because it validates solutions in the finding space simultaneously. GA has the ability to deliver a good-enough and a fast-enough solution. This makes GA attractive for use in solving optimization problems. It is possible to apply these advantages of GA to improve the limitations of ANN. This technique in which the ANN and GA are integrated is called GANN method (Ahmad et al., 2010; Sangwan et al., 2015). GANN processing algorithm is illustrated in Fig. 2. It should be noted that the best structure for the ANN and GA is chosen based on the feedback received from the network.

5. Coulomb stress change

The coulomb stress change is a seismic process, whose origin is a local discrete deformation event. It indicates that stress during an earthquake can cause movements in some parts of the fault and it is used in earthquake-forecasting models to assess earthquake activity.

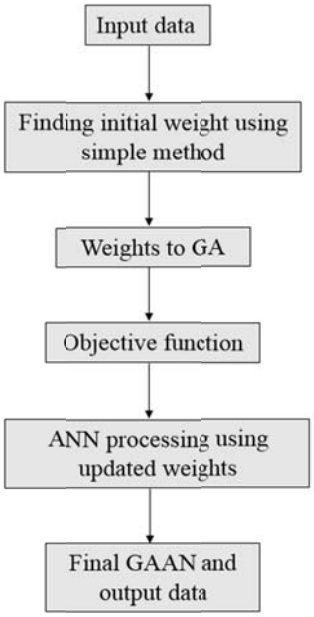

Figure 2. Sequence of operations in the integrated method of GANN.

The coulomb stress change caused by the earlier earthquakes can explain the epicenter location of aftershocks. The aftershocks probably occur in that location where the coulomb stress exceeds the failure strength of the fault surface. The change of coulomb failure stress can be defined as (Cocco and Rice, 2002; Wang et al., 2014):

$$\Delta CFF = \Delta\tau + \mu\left(\Delta\sigma_n + \Delta P\right) \tag{4}$$

where $\Delta\tau$ is the shear stress in the direction of slip on the fault plane, μ is the friction coefficient, $\Delta\sigma_n$ is its normal stress change and ΔP is the pore pressure change. During the co-seismic phase, the pore pressure change can be expressed as (Cocco and Rice, 2002; Wang et al., 2014):

$$\Delta P = -B\frac{\Delta\sigma_{kk}}{3} \tag{5}$$

where $\Delta\sigma_{kk}$ is the trace of the stress change tensor, and B is Skempton's coefficient. As a result, the coulomb failure model may be written as (Cocco and Rice, 2002; Wang et al., 2014):

$$\Delta CFF = \Delta\tau + \mu\left(\Delta\sigma_n - B\frac{\Delta\sigma_{kk}}{3}\right) \tag{6}$$

Considering the fault parameters, the coulomb stress change for co-seismic deformation can be expressed as (Cocco and Rice, 2002; Wang et al., 2014):

$$\begin{aligned}\Delta CFF = {} & \sin\lambda[-\frac{1}{2}\sin^2\phi\sin(2\delta)\sigma^{11} + \frac{1}{2}\sin(2\phi)\sin(2\delta)\sigma^{12} + \sin\phi\cos(2\delta)\sigma^{13} \\ & -\frac{1}{2}\cos^2\phi\sin(2\delta)\sigma^{22} - \cos\phi\cos(2\delta)\sigma^{23} + \frac{1}{2}\sin(2\delta)\sigma^{33}] \\ & + \cos\lambda[-\frac{1}{2}\sin(2\phi)\sin\delta\sigma^{11} + \cos(2\phi)\sin\delta\sigma^{12} + \cos\phi\cos\delta\sigma^{13} \\ & + \frac{1}{2}\sin(2\phi)\sin\delta\sigma^{22} + \sin\phi\cos\delta\sigma^{12}] + \mu[\sin^2\phi\sin^2\delta\sigma^{11} - \sin(2\phi)\sin^2\delta\sigma^{12} \\ & - \sin\phi\sin(2\delta)\sigma^{13} + \cos^2\phi\sin^2\delta\sigma^{22} + \cos\phi\sin(2\delta)\sigma^{23} + \cos^2\delta\sigma^{33} - \frac{B}{3}(\sigma^{11} + \sigma^{22} + \sigma^{23})]\end{aligned} \tag{7}$$

where ϕ, λ and δ are the strike, rake and dip angle of the fault and $\{\sigma^{ij} \mid i, j = 1,2,3\}$ are the components of the stress change tensor. Previous experiments and studies concluded that the values of μ are between 0.6 and 0.8 for most rock materials (Byerlee, 1978; Cattin et al., 2009). Besides, Skempton's coefficient is between 0.4 and 0.9 for granite, sandstone and marble, but still unconstrained for other rocks. In this study, according to the geological features of the study area, the values of μ' and B are considered to be equal to 0.6 and 0.5 respectively (Byerlee, 1978; Cattin et al., 2009; Khodaverdian et al., 2015).

6. Data set

To perform the InSAR analysis, the two Sentinel-1A radar acquisitions are used. The dates of acquisitions are very near to the date of Sefid-Sang earthquake that enables better quantification of co-seismic displacement. The features of data can be seen in Table 1.

7. Numerical results and discussion

In this section, the focus is on the case study of the paper, presenting the numerical results and detailed analysis of Sefid-Sang earthquake along with its fault system. At the outset, we about the selected SAR acquisitions and the earthquake deformation field extracted from them are briefly discussed. In the next step, an inversion problem is conducted to determine the fault parameters using Okada (1985) model by integration of the genetic algorithm with the artificial neural network.

7-1. Processing of radar acquisitions and earthquake displacement field

The open source and free InSAR processing software GMTSAR is prepared in c-code and csh scripts (Sandwell et al., 2011). This software provides the possibility to easily process SAR, to access to the relevant code and to add some filters in order to enhance the accuracy of the final displacement fields. InSAR processing initiates with the preprocessing step from radar data using DEM and orbital information. The interferograms are multi-looked by a factor 6 in range and 4 in azimuth, and the Lee filter is used for phase filtering. Fig. 3 shows the interferograms of ascending and descending passes. Fig. 4 shows the horizontal and vertical components of displacement field derived by combination of descending and ascending interferograms.

As can be seen in Fig. 4, the maximum observed vertical displacement is about 12 cm and the maximum horizontal displacement is about 4 cm occurred around the fault region.

Table 1. Sentinel-1A acquisitions.

Mission	Master Date	Slave Date	Pass	Perpendicular Baseline (m)	Look Angle (d)
Sentinel- 1A	2017/03/25	2017/04/10	D	27	32
Sentinel- 1A	2017/03/28	2017/04/08	A	31	43

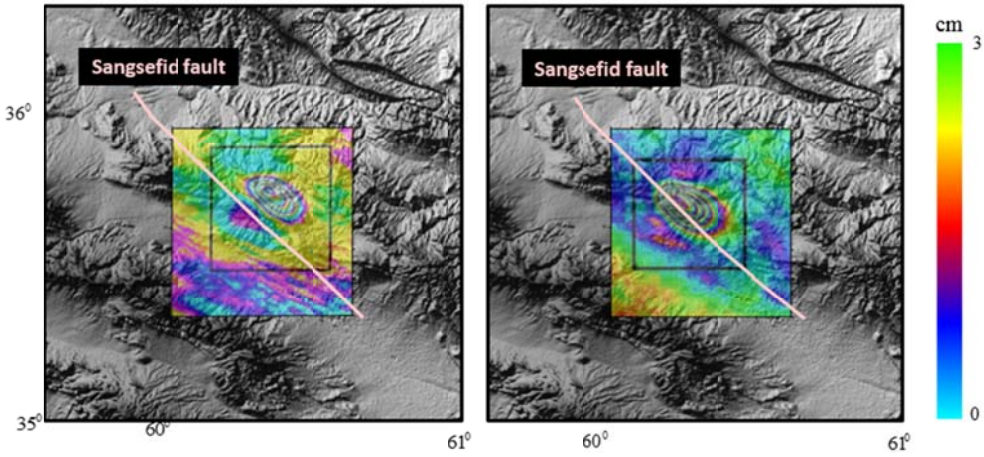

Figure 3. The obtained interferograms (left: Ascending and right: descending).

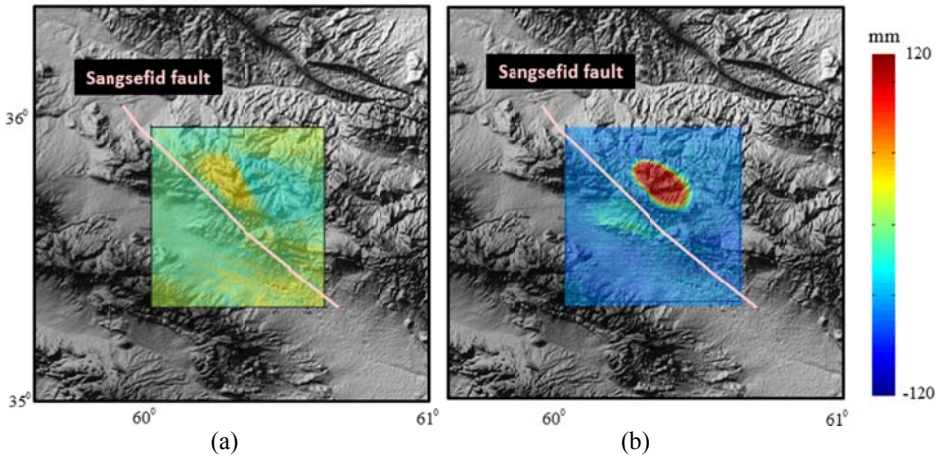

Figure 4. 3D map of horizontal (a) and vertical (b) displacement fields.

7-2. Inversion of displacement field to focal mechanism and fault parameters

In this section, the optimum fault parameters and focal mechanism of Sefid-Sang fault system are computed using the inversion of the displacement field. The fault parameters include length, width, dip angle, strike, rake, depth and slip vector. In order to achieve the training settings and evaluate the performance of the trained artificial neural network, the use of simulated data is necessary. The training data is prepared by changing parameters in the specific limits. Parameter ranges and rates of change can be seen in Table 2.

A fixed artificial neural network for all samples which consists of 4812 points is considered. Introducing the sample fault parameters as an input to the Okada model, the displacement field is calculated and used as an input to the ANN. Therefore, ANN has 4812 inputs and 5 output neurons; therefore, 3670 samples are prepared. 2120 samples are used for training of artificial neural network, and 1550 samples are used to evaluate the network. Here, GA is applied to adjust the weights of the network connections. The Mean Square Error (MSE) is used to evaluate the network performance. The computations are completed when the MSE tends to a constant value. After the training step, the deformation field derived from InSAR observations is used as an input for GANN, and the fault parameters are derived as an output. The results for fault parameters are shown in Table 3. Consequently, moment magnitude of about 5.7 Mw scale is computed for this earthquake.

The computed parameters for this fault using different data sets are presented in Table 4. As can be seen, the results of this study are close to the results obtained from different methods and data sets. Existing differences are because other data sets considered the fault as a point, and so do not provide a fault dimension. Moreover, these differences are existed between these other data sets.

Table 2. Parameter ranges and rates of change.

	Locking depth (km)	Dip angle (deg)	Width (km)	Length (km)	Strike (deg)	Rake (deg)	Slip (m)
Limit	5-10	55-75	8-16	20-40	110-150	0-60	0.5-6.5
Rate of changes	1	10	2	2	10	10	0.5

Table 3. The results of the calculation of fault parameters and their standard deviation.

	Locking depth (km)	Dip angle (deg)	Width (km)	Length (km)	Strike angle (deg)	Rake angle (deg)	Slip (m)
Result	8	55	10	34	210	154	4.5
Standard deviation	1.3	4.7	2.1	3.4	3.8	1.9	0.78

7-3. Coulomb strain and stress computation

In this section, the strain and stress are calculated using the Coulomb model and also the dilatation caused by the earthquake deformation is derived. The stress and strain are calculated using the final fault parameters determined in the previous section. Fig. 5 (a)–(c) represents the three components of the normal strain and Fig. 5(d)–(f) represents the components of the shear strain S_{xy}, S_{Yz} and S_{Xz} lying in the XY, XZ and YZ planes, respectively, thereby denoting the propagation of strain energy along the north-west–south-east direction.

Fig. 6 shows the pattern of coulomb stress change. According to this figure, one can infer that at first the compressive stress is occurred, and then the tensile stress is prevailed. With a careful looking, the results expressed itself in dilatation. In Fig. 6, red color represents regions of increased stress, and blue represents regions of decreased stress.

Table 4. Fault parameters estimated from different data sets.

Data set	Locking depth (km)	Dip angle (deg)	Width (km)	Length (km)	Strike angle (deg)	Rake angle (deg)	Slip (m)
USGS	13	20.73	-	-	316.105	127.58	-
GCMT	12	53.44	-	-	312.91	117.59	-
IRSC	6	45.46	-	-	329.101	120.80	-

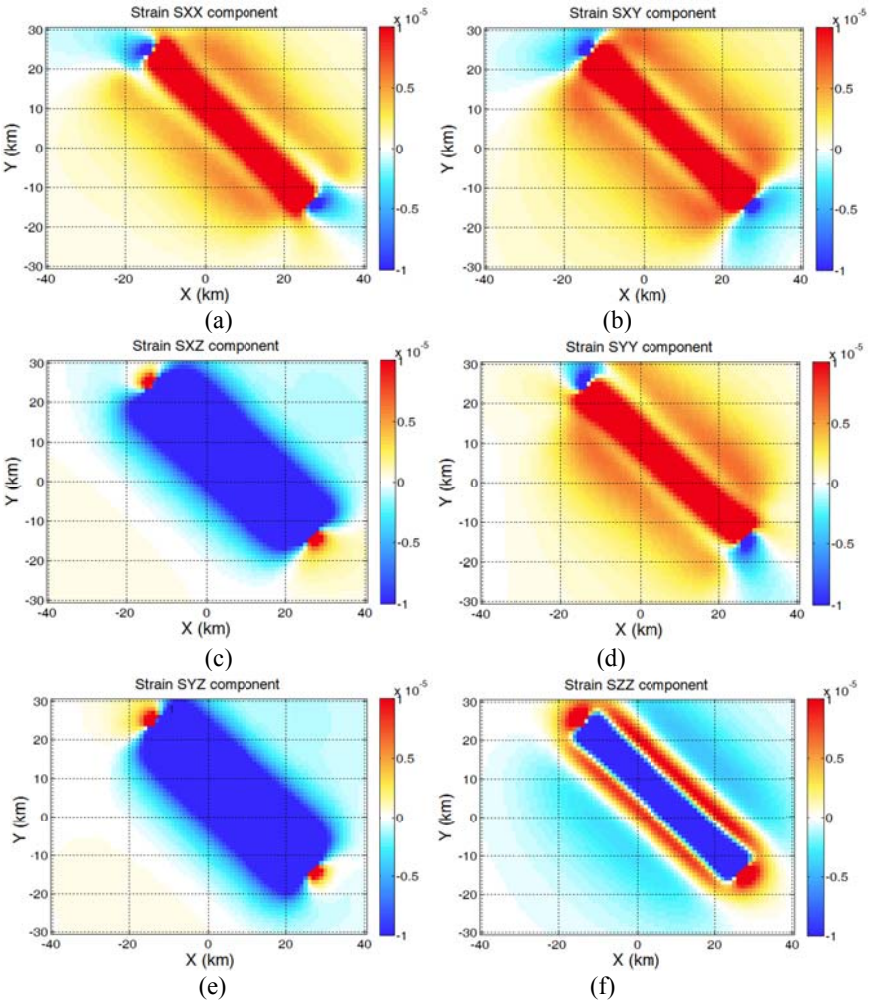

Figure 5. The coulomb strain field. Normal Strain produced along the (a) x-direction (b) y-direction (c) z-direction and the shear strain produced in the (d) XY plane (e) YZ plane (f) XZ plane (positive change denoted by red and negative by blue colour).

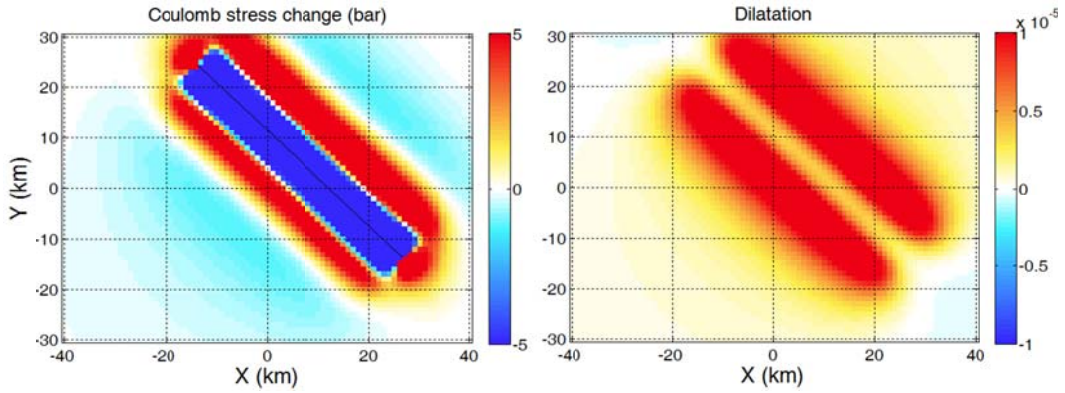

Figure 6. The coulomb stress change and dilatation from coulomb model.

8. Conclusion

In this study, the source parameters of Sefid-Sang earthquake have been determined using the InSAR technique of co-seismic deformation field acquired by Sentinel-1A satellite. To do so, two acquisitions before and two acquisitions after the earthquake are compared to each other to derive the LOS displacement fields in directions of ascending and descending tracks. Moreover, using both descending and ascending LOS displacement fields, the 3D displacement field in the local coordinate system is derived. Finally, the nonlinear inversion problem is conducted to constrain the fault parameters using the observed surface displacement field with the aid of artificial neural network optimization method, equipped with genetic algorithm. The results of inversion process for fault depth and slip are 8 km and 4.5 m respectively. Besides, moment magnitude of about 5.7 Mw is computed for this earthquake.

Acknowledgments

Authors would like to appreciate the European Space Agency (ESA) for providing the radar acquisitions.

References

Ahmad, F., Mat-Isa, N., Hussain, Z., Boudville, R. and Osman, M., 2010, Genetic Algorithm-Artificial Neural Network (GA-ANN) hybrid intelligence for cancer diagnosis. Proceedings of the 2nd International Conference on Computational Intelligence, Communication Systems and Networks (CICSYN '10), pp. 78.

Akbari, M., Ghafoori, M. Moghaddas, N. H. and Lashkaripour, G. R., 2011, Seismic microzonation of Mashhad city, northeast Iran, Annals of Geophysics, 54(4), 424-434.

Ambraseys, N. N. and Melville, C. P., 1982, A History of Persian Earthquakes, Cambridge University Press, Cambridge, UK, 219 pp.

Byerlee, J., 1978, Friction of rocks, Pure Appl. Geophys., 116, 615–626.

Cattin, R., Chamot-Rooke, N., Pubellier, M., Rabaute, A. Delescluse, M. Vigny, C. Fleitout, L. and Dubernet, P., 2009, Stress change and effective friction coefficient along the Sumatra-Andaman-Sagaing fault system after the 26 December 2004 (Mw = 9.2) and the 28 March 2005 (Mw = 8.7) earthquakes, Geochem. Geophys. Geosyst., 10, Q03011, doi:10.1029/2008GC002167.

Cocco, M. and Rice, J. R., 2002, Pore pressure and poroelasticity effects in Coulomb stress analysis of earthquake interactions, J. Geophys. Res., 107(B2), 2030, doi:10.1029/2000JB000138.

Del Frate, F., Ferrazzoli, P. and Schiavon, G., 2003, Retrieving soil moisture and agricultural variables by microwave radiometry using neural networks. Remote Sens. Environ, 84:174–183.

Del Frate, F. and Salvatori, L., 2004, Oil spill detection by means of neural network algorithms: a sensitivity analysis. Proceedings of the Geoscience and Remote Sensing Symposium, IGARSS '04. Anchorage (AK): IEEE International, 2, 1370--1373.

Fattahi, H. and Amelung, F., 2016, InSAR

observations of strain accumulation and fault creep along the Chaman Fault system, Pakistan and Afghanistan. Geophysical Research Letters, 43(16): 8399–8406.

Fialko, Y., Simons, M. and Agnew, D., 2001, The Complete (3-D) Surface Displacement Field in the Epicentral Area of the 1999 M(W) 7.1 Hector Mine Earthquake, California, from Space Geodetic Observations. Geophysical Research Letters, 28(16), 3063–3066. doi:10.1029/2001GL013174.

Furuya, M. and Satyabala, S. P., 2008, Slow earthquake in Afghanistan detected by InSAR, Geophys. Res. Lett., 35(6), doi:10.1029/2007GL033049.

Goldberg, D. E., 1989, Genetic Algorithms in Search, Optimization and Machine Learning. Addison-Wesley Publishing Co., Reading, Massachusetts, 412 pp. 17. Han, S.C., Shum, C.K., Bevis, M., Ji C., Kuo, C.Y., 2006. Crustal dilatation.

Guangyu Xu., Caijun Xu., Yangmao Wen., 2018, Sentinel-1 observation of the 2017 Sangsefid earthquake, northeastern Iran: Rupture of a blind reserve-slip fault near the Eastern Kopeh Dagh. Tecto, doi:10.1016/j.tecto.2018.03.009.

Haji-Aghajany, S., Voosoghi, B. and Yazdian, A., 2017, Estimation of north Tabriz fault parameters using neural networks and 3D tropospherically corrected surface displacement field. Geomatics, Natural Hazards and Risk. doi.org/10.1080/19475705.2017.1289248.

Haupt, R. L and Haupt, S. E., 2004, Practical Genetic Algorithms, 2nd Edition, John Wiley & Sons Inc.

Huadong, G., Xinyuan, W., Xinwu, L., Guang, L., Lu, Z. and Shiyong, Y., 2010, Yushu earthquake synergic analysis study using multi-modal SAR datasets. Chinese Science Bulletin, 55(31), 3499–3503.

Jolivet, R., Lasserre, C., Doin, M., Guillaso, S., Peltzer, G., Dailu, R., Sun, J., Shen, Z. and Xu, X., 2012, Shallow creep on the Haiyuan Fault (Gansu, China) revealed by SAR Interferometry. Journal of Geophysical Research, 117, http://dx.doi.org/10.1029/2011JB008732.

Kaneko, Y., Fialko, Y., Sandwell, D. T., Tong, X. and Furuya, M., 2013, Interseismic deformation and creep along the central section of the North Anatolian Fault (Turkey): InSAR observations and implications for rate-and-state friction properties, J. Geophys. Res. Solid Earth, 118(1), 316–331, doi:10.1029/2012JB009661.

Kawasaki, I., Asai, Y., Tamura, Y., Sagiya, T., Mikami, N., Okada, Y., Sakata, M. and Kasahara, M., 1995, The 1992 Sanriku-Oki, Japan, ultraslow earthquake, J. Phys. Earth, 43, 105–116.

Khodaverdian, A., Zafarani, H. and Rahimian, M., 2015, Long term fault slip rates, distributed deformation rates and forecast of seismicity in the Iranian Plateau, Tectonics, 34, 2190–2220, doi:10.1002/2014TC003796.

Michalewicz, Z., 1992, Genetic Algorithm+ Data Structures =Evolution Programs. Springer Verlag, Berlin, 340 pp.

Maruyama, T., 1964, Statical elastic dislocation in an infinite and semi-infinite medium. Bull Earthq. Res. Inst., 42, 289-368.

Motagh, M., Bahroudi, A., Haghighi, M. H., Samsonov, S., Fielding, E. and Wetzel, H.U., 2015, The 18 August 2014 Mw 6.2 Mormori, Iran, Earthquake: A thin - skinned faulting in the Zagros Mountain inferred from InSAR measurements. Seismological Research Letters, 86(3), 775–782.

Okada, Y., 1985, Surface deformation due to shear and tensile faults in a half-space. Bull. Seism. Soc. Am., 75, 1135-1154.

Sandwell, D., Mellors, R., Tong, X., Wei, M. and Wessel, P., 2011, An InSAR Processing System Based on Generic Mapping Tools. Scrips Institution of Oceanography Technical Report, University of California, San Diego.

Sangwan, K., Saxena, S. and Kant, G., 2015, Optimization of machining parameters to minimize surface roughness using integrated ANN-GA approach. Proceedings of the 22nd CIRP Conference on Life Cycle Engineering (LCE '15), 29, 305–310, Sydney, Australia.

Steketee, J. A., 1958a, On Volterra's dislocations in a semi-infinite elastic medium. Can. J. Phys., 36, 192–205.

Steketee, J. A., 1958b, Some geophysical applications of the elasticity theory of dislocations. Can. J. Phys., 36, 1168–

1198.

Walker, R., Jackson, J. and Baker, C., 2003, Thrust faulting in eastern Iran: source parameters and surface deformation of the 1978 Tabas and 1968 Ferdows earthquake sequences, Geophys. J. Int., 152, 749–765.

Wang, X. P. and Cao, L. M., 2002, Genetic Algorithm: Theory, Application and Software, Xian Transportation University Press, Xian.

Wang, R. J., Parolai, S., Ge, M. R., Jin, M. P., Walter, T. R. and Zschau, J., 2013, The 2011 M-w 9.0 Tohoku Earthquake: comparison of GPS and Strong-Motion Data. Bull. Seismol. Soc. Am., 103, 1336–1347. doi: 10.1785/0120110264.

Wang, J., Xu, C., Freymueller, J. T., Li, Z., and Shen, W., 2014, Sensitivity of Coulomb stress change to the parameters of the Coulomb failure model: A case study using the 2008 Mw 7.9 Wenchuan earthquake, J. Geophys. Res. Solid Earth, 119, 3371–3392, doi:10.1002/ 2012JB009860.

Xu, C., Liu, Y., Wen, Y. M. and Wang, R., 2010, Coseismic slip distribution of the 2008 mW 7.9 Wenchuan earthquake from joint inversion of GPS and InSAR Data. Bull. Seis. Soc. Am., 100, 2736–2749, doi: 10.1785/0120090253.

Yang, J. G., Weng, S. Y. and Zhao, H., 2001, Applied Textbook of Artificial Neural Network, Zhejiang University Press, Hangzhou.

Zebker, H. A. and Villasenor, J., 1992, Decorrelation in interferometric radar echoes. IEEE Transactions on Geoscience and Remote Sensing, 30(5), 950– 959.

Zell, A., Mamier, G., Vogt, M., Mache, N., Hubner, R., Doring, S., Herrmann, K.U., Soyez, T., Schmalzl, M. and Sommer, T., 1995, SNNS, Stuttgart Neural Network Simulator, User Manual, Version 4.1. Stuttgart: Institute for Parallel and Distributed High Performance Systems, University of Stuttgart.